Sensitivity of last glacial maximum climate to sea-ice conditions in the Nordic Seas

ØYVIND BYRKJEDAL[1] (✉)

Bjerknes Centre for Climate Research, University of Bergen, Allegaten 55, 5007 Bergen, Norway

Geophysical Institute, University of Bergen, Allegaten 70, 5007 Bergen, Norway

NILS GUNNAR KVAMSTØ

Geophysical Institute, University of Bergen, Allegaten 70, 5007 Bergen, Norway

Bjerknes Centre for Climate Research, University of Bergen, Allegaten 55, 5007 Bergen, Norway

MARIUS MELAND

Bjerknes Centre for Climate Research, University of Bergen, Allegaten 55, 5007 Bergen, Norway

Department of Earth Science, University of Bergen, Allegaten 41, 5007 Bergen, Norway

EYSTEIN JANSEN

Bjerknes Centre for Climate Research, University of Bergen, Allegaten 55, 5007 Bergen, Norway

Department of Earth Science, University of Bergen, Allegaten 41, 5007 Bergen, Norway

[1] Corresponding Author:

Email: Oyvind.Byrkjedal@bjerknes.uib.no, phone: 47-55582594, fax 47-55589883

Abstract

Published reconstructions of Last Glacial Maximum (LGM) sea surface temperatures and sea ice extent differ significantly. We here test the sensitivity of simulated North Atlantic climates to two different reconstructions by using these reconstructions as boundary conditions for model experiments. An atmospheric general circulation model has been used to perform two simulations of the Last Glacial Maximum and a modern-day control simulation. Standard (CLIMAP) reconstructions of sea ice and sea surface temperatures have been used for the first simulation, and a set of new reconstructions in the Nordic Seas/Northern Atlantic have been used for the second experiment. The new reconstruction is based on 158 core samples, and represents ice-free conditions during summer in the Nordic Seas, with accordingly warmer sea surface temperatures and less extensive sea ice during winter as well. The simulated glacial climate is globally 5.7K colder than modern day, with the largest changes at mid and high latitudes. Due to more intense Hadley circulation, the precipitation at lower latitudes has increased in the simulations of the LGM. Relative to the simulation with the standard CLIMAP reconstructions, reduction of the sea ice in the North Atlantic gives positive local responses in temperature, precipitation and reduction of the sea level pressure. Only very weak signatures of the wintertime Icelandic Low occur when the standard CLIMAP sea surface temperature reconstruction is used as the lower boundary condition in LGM. With reduced sea ice conditions in the Nordic Seas, the Icelandic Low becomes more intense and closer to its present structure. This indicates that thermal forcing is an important factor in determining the strength and position of the Icelandic Low.

The Arctic Oscillation is the most dominant large scale variability feature on the Northern Hemisphere in modern day winter climate. In the simulation of the LGM with extensive sea ice this pattern is significantly changed and represents no systematic large scale variability over the North Atlantic. Reduction of the North Atlantic sea ice extent leads to stronger variability in monthly mean sea level pressure in winter. The synoptic variability appears at a lower level in the simulation when standard reconstructions of the sea surface in the LGM are used. A closer inspection of storm tracks in this model experiment shows that that the synoptic lows follow a narrow band along the ice edge during winter. The trajectories of synoptic lows are not constrained to the sea ice edge to the same degree when the sea ice extent is reduced. Seasonally open waters in the Nordic Seas in the new reconstruction apparently act as a moisture source, consistent with the current understanding of the rapid growth of the Fennoscandian and Barents Ice Sheets, during the Last Glacial Maximum. The signal from the intensified thermal forcing in the North Atlantic in Boreal winter is carried zonally by upper tropospheric waves, and thus generates non-local responses to the changed sea ice cover.

1 Introduction

The state of the sea surface in the Arctic, North Atlantic and Nordic Seas provides important constraints on the climate in Europe and Eurasia, and strongly influence the strength of the Atlantic meridional overturning circulation (Bentsen et al. 2004). The reliability of reconstructions of past climate states is crucial for developing a physical understanding of past climate changes, their dynamics, magnitude and underlying driving mechanisms. Reliable sea surface reconstructions are also critical as boundary conditions for Atmospheric General Circulation Model (AGCM) experiments of the Last Glacial Maximum (LGM) and as data for validation of experiments with fully coupled GCMs.

The global LGM reconstruction of CLIMAP (1981) which has frequently been used as LGM boundary conditions has been heavily debated. Numerous studies (e.g. Dong and Valdes 1998; Shin et al. 2003) concluded that the CLIMAP sea ice reconstruction in the Northern Hemisphere is too extensive. However, due to lack of alternatives, the CLIMAP reconstruction has been commonly used as boundary conditions for AGCM simulations of LGM (e.g. Kutzbach 1988; Lautenschlager and Herterich 1990; Hall et al. 1996). In the high-latitude North Atlantic and the Nordic Seas this reconstruction suggests permanent sea ice cover as far south as 45˚N, also in the summer. New evidence, however, clearly indicates larger areas of at least seasonally open waters (e.g. Veum et al. 1992; e.g. Hebbeln et al. 1994; Wagner and Henrich 1994; Sarnthein et al. 1995; Weinelt et al. 1996). The difference between a perennially frozen ocean and an open or seasonally open ocean has wide climatic implications. For example, as the marginal ice zone heavily influences the low level baroclinicity, the equatorward shift during LGM may have had a significant impact on mid latitude storm tracks and the associated heat and moisture transport. This could in turn result in large consequences for the growth and maintenance of the high latitude ice sheets and deep water formation with the associated meridional overturning circulation. Renewed attempts to better constrain the state of the LGM surface of the Nordic Seas and the northern North Atlantic have therefore been pursued. New estimates of sea surface temperatures (SST) showing seasonally open waters in the Nordic Seas, have previously been

published, based on foraminiferal species distributions (e.g. Pflaumann et al. 1996; Pflaumann et al. 2003), alkenones (Rosell-Mele and Comes 1999) and dinocyst assemblage methods (de Vernal et al. 2000).

Common for all new attempts to reconstruct the LGM surface ocean in the North Atlantic/Nordic seas by proxy methods is that they indicate warmer temperatures and less sea ice in the Eastern and Central Nordic Seas than the CLIMAP reconstruction. Thus to test the sensitivity of simulated atmospheric circulation to the choice of surface ocean boundary reconstructions, would for all available reconstructions involve a reconstruction with less sea ice and a higher temperature than the CLIMAP reconstruction. It is also well known that all paleoclimate proxy methods have problems of reconstructing the cold end member. Similarly, the seasonality of LGM climates is difficult to assess with high confidence since most proxies are calibrated against summer conditions. The low planktic foraminifer diversity in the polar water masses make the SST estimates, based on planktic foraminiferal transfer functions, unreliable when summer temperatures are below 4-5°C. The alkenone and dinocyst assemblage methods have also similar difficulties and probably larger problems in the low temperature end. In the study area the LGM reconstructions from these two methods (Rosell-Mele and Comes 1999, de Vernal et al. 2000) show a high scatter. In some cases they also show temperatures that are much too high to be reasonable given the temperature constraints we have from O-isotopes. We have thus not considered these results for our experiments.

Meland et al. (2005) used a different approach and produced an SST-reconstruction based on the O-isotope ratios of planktic foraminiferal calcite. The O-isotopic fractionation is dependant on ambient temperature, but the isotopic composition is also influenced by sea water salinity (see e.g. Meland et al, 2005 for details) which needs to be accounted for before SSTs can be calculated. Meland et al. (2005) used various approaches to constrain the potential salinity component of the LGM O-isotope distribution and arrive at an SST reconstruction which in broad aspects is quite similar to the one based on the foraminifer transfer function method of Pflaumann et al. (1996), but with a more reasonable zonal gradient and slightly lower SSTs inside the Nordic Seas. For the present paper

choosing this reconstruction rather than that of Pflaumann et al. (1996) would probably not change the results by much. Both reconstructions are based on a large data set and have a very consistent regional pattern with almost no outlier values. The O-isotope reconstruction has some advantages, as it does not have an end-member effect as long as salinity can be reasonably assessed, thus it provides a wider range of SSTs in the Nordic Seas than the foraminifer transfer functions which gives a reconstruction without any zonal temperature gradient between Scandinavia and Greenland, a situation which is unlikely. We have thus selected the reconstruction of Meland et al. (2005) as lower boundary for the experiments with the ARPEGE atmospheric general circulation model (Deque et al. 1994; Deque and Piedelievre 1995; Deque et al. 1998). The SST estimates in the new reconstruction are based on oxygen isotopes of the planktonic foraminifer *Neogloboquadrina pachyderma* sinistral. The gridded data set is based on interpolation of 158 core locations, covering the northern North Atlantic and the Nordic Seas. For this reconstruction the LGM is defined as the period 18.0 - 21.5 cal. ka BP (15 - 18 14C ka), in agreement with the definition of the Glacial Atlantic Ocean Mapping (GLAMAP 2000) LGM time slice (Pflaumann et al. 2003). This period is, based on oxygen isotope records from the Nordic Seas, known to be a period of stability and minimum melt water influx (Sarnthein et al. 1995).

In order to identify the impact of extended open waters in the Nordic Seas on the general circulation during LGM, a standard LGM experiment according to the Paleoclimate Modelling Intercomparison Project (PMIP) protocols (Joussaume and Taylor 1995; Joussaume and Taylor 2001) has been carried out with ARPEGE. This experiment uses the CLIMAP (1981) SST reconstruction for LGM. CLIMAP defined LGM as the youngest distinct carbonate minimum prior to Termination 1. We assume here that these values are within the GLAMAP 2000 definition of LGM.

In section 2 the experimental setup is explained. Section 3 gives an overview of the simulated climatology of LGM in comparison to the control simulation. The variability of the simulated LGM climate is discussed in terms of empirical orthogonal function (EOF) analysis and storm tracks in section 4. The response to

the modified reconstruction of SST and sea ice is described and discussed in section 5. Conclusions are given in section 6.

2 Experimental design

The atmospheric general circulation model, ARPEGE (Deque et al. 1994; Deque and Piedelievre 1995; Deque et al. 1998) is set up for 3 experiments. The horizontal resolution is given by a spectral truncation at wave number 63 (T63), and a grid spacing of approximately 2.8° in latitude and longitude. The model is divided into 31 vertical layers, 21 layers in the troposphere and 10 in the stratosphere. Each experiment is run for 15 years; the analysis will focus on the last 10 years, thus allowing the model a spin-up period of 5 years.

The first experiment is the control (CTL) run where modern day vegetation, topography, and insolation are used. Climatological SSTs and sea-ice distribution (Reynolds and Smith 1995) for February and August are used to construct a sinusoidal annual cycle. CTL is run with modern day levels of greenhouse-gases (345 ppm CO_2, 1750ppb CH_4, 310 ppb N_2O) and aerosols. This experiment is designed according to PMIP (Bonfils et al. 1998).

The second experiment is a standard LGM run (LGM_S). Glacial values for the atmospheric constituents are used; 200 ppm CO_2, 350 ppb CH_4, 190 ppb N_2O, no aerosols. The LGM climate was very different from modern day climate, but the insolation 21,000 calendar years ago was quite similar. Insolation on top of the atmosphere was less than 2% weaker at the poles, averaged over the year, compared with modern day, while insolation at the equator was approximately 0.2% stronger. Modern day orbital parameters are a good approximation to LGM insolation, and are used in our LGM simulations. The arbitrarily constructed annual cycle constitute a larger uncertainty to the annual cycle than the orbital parameters. The SSTs and sea-ice distribution are taken from CLIMAP (1981). The CLIMAP paleo-reconstructions give a climatological global dataset of SST and sea-ice for LGM, where the months of February and August define the range of the annual, and in this case, sinusoidal cyclicity.

In LGM large ice sheets covered Scandinavia and possibly the Barents- and Kara-seas. These ice sheets were thick and reached about 2km above sea level (Peltier 1994). Large amounts of present ocean water were bound up in these ice sheets, and thus, glacial sea level was lower than present. The more than 3 km thick Laurentide ice sheet covered northern parts of eastern North America down to 40°N. The Cordilleran ice sheet was situated on the western side of the Rockies. The description of land ice and topography which have been used as boundary condition for LGM is given in Peltier (1994).
The total amount of excess ice volume in LGM is estimated to be 55-64 million km^3 (Denton and Hughes 1981). The sea level is estimated to be 109-129 m lower in LGM. The reduced sea-level uncovers new land areas that are presently under water e.g. in the Indo-pacific region. However, in this study the modern land/sea mask and sea levels are employed. In the region of interest, the change in sea level is small compared to the changes in topography (Peltier 1994). The focus here is directed more regionally to the mid and high latitudes in the northern hemisphere where land-sea changes plays a minor role compared to the land ice and topography differences. In the LGM_S experiment, the North Atlantic is covered by sea ice north of 45°N in February, but opens up during spring and summer to the minimum ice-extent in August, when an area of open water is found west of Ireland.

The third experiment is a new LGM simulation (LGM_N). The set of new SST reconstructions published by Meland et al.(2005) is applied. Meland et al. (2005) have reconstructed the SSTs based on 158 core samples, and suggest that the summer extent of sea ice is more similar to present, with open ocean in the Nordic Seas. In this study it is assumed that the reconstruction of Meland et al. (2005) represents the temperature of the sea surface in August in LGM. The sea ice cover in August is defined by the -0.5ºC isotherm. Based on the summer SSTs from the Meland et al. (2005) reconstruction we have fitted a reasonable seasonal range based on the seasonal range of SSTs at present in the area for the same temperature at each grid point. During winter an area of open water is present west of Ireland, but the sea ice cover is otherwise similar to the CLIMAP (1981) reconstruction. See figure 1 for the CLIMAP (1981) and Meland et al. (2005) reconstructions in the North Atlantic.

3 Simulated climatology of standard LGM (LGM_S)

3.1 Mass

Figure 2 shows the zonally averaged annual mean sea level pressure (MSLP) differences between the CTL and LGM_S simulations. For comparison, corresponding data are included from 9 other similar experiments from PMIP (Joussaume and Taylor 1995; Joussaume and Taylor 2001), which all have been run with prescribed boundary conditions from CLIMAP for LGM and modern day. The models divide into two clusters. In one cluster global pressure increases ~10-12hPa in the LGM climate. This is due to the way the 110m reduction in sea level is treated in those models. In the second cluster, in which our model is contained, there is a negligible change in global mean pressure. If a constant pressure value of 10-12hPa is removed from the first cluster, the model outputs have similar zonal MSLP response to the external LGM forcing.

Similar to the 9 PMIP models ARPEGE show an increase in pressure north of ~40ºN from present to LGM, and a slight reduction in pressure in the tropics between 30ºN and 30ºS. Around 50ºS there is a pressure increase which gradually drops to a significant reduction in the Antarctic region. There is a large spread between the models concerning the southernmost areas (south of ~75ºS).

The geographical distribution of changes in mean sea level pressure (MSLP) is shown in figure 3. The changes shown are all significantly different from zero at the 1% level. One of the most striking features of the MSLP changes in Boreal winter (figure 3a) is the large increase in MSLP over the North Atlantic and Europe. This represents an intensified Siberian high during LGM which has merged with the strengthened high pressure over southern Europe, Northern Africa, the Middle East and the Caspian Sea. The southern part of this high pressure area during LGM in winter is associated with an intensified Hadley circulation, while the northern Siberian part is linked to reduced storm track activity in the Atlantic and Eurasian regions. The latter feature is indicated by the substantial reduction of the Icelandic Low in LGM_S. The Aleutian Low west of Alaska and south of the Bering Strait is strengthened and its centre is moved

eastward to the Gulf of Alaska. This is seen as an increase in MSLP in the Sea of Okhotsk and a large reduction in the Gulf of Alaska. Pressure is in general increased over the Arctic. Consistent with the zonal mean data, pressure is decreased along the equator and south, with the strongest decrease over the African and South American continents. Simulated pressure changes between CTL and LGM_S in Austral winter (figure 3b) are relatively symmetric to those in Boreal winter. However, the intensified sub-tropical highs and more intensified mid-latitude circumpolar low have a far more zonal character than the corresponding features in the Northern Hemisphere. The circumpolar Southern Ocean low propagates to a larger extent into the Antarctic in Austral winter in LGM_S compared to CTL. The most noticeable Northern Hemispheric feature in this season is the higher MSLP over the continents and North Atlantic in LGM_S. In particular, a prominent high pressure over the Scandinavian, Barents and Kara ice sheets is apparent. A reduction in MSLP over the north Pacific is also found.

The Hadley cell (not shown) is more vigorous in LGM_S during Boreal winter. This is consistent with the reduced tropical and increased sub-tropical MSLP in LGM_S in this season. During Boreal summer the situation is reversed and the Hadley cell is slightly less intense in LGM_S than in CTL. This is expected since northern hemisphere land masses are cooled by the extended LGM ice sheets and thus are less able to heat surface air that enters the updraft regions from northern continental areas.

3.2 Precipitation

The annual globally averaged precipitation in CTL is 3.07 mm/day. The other PMIP models have global means of 2.7-3.2 mm/day in their modern day simulations. With respect to simulated LGM climate, globally averaged precipitation is 3.58 mm/day in LGM_S, while the nine other PMIP-models have precipitation within the range 2.5-2.9 mm/day. The intermodel spread is larger for the LGM simulations than for simulations of modern day climate. However, ARPEGE is the only model that experience increased precipitation in LGM. Figure 4 shows the difference in precipitation between LGM_S and CTL. On average precipitation is increased in the tropics and subtropics during both

seasons. In Boreal winter, increase in precipitation over eastern South America, south eastern Africa and the Indian Ocean in LGM_S is specifically pronounced. This is in the rising part of the Hadley cell and thus consistent with the above mentioned increase in the LGM Hadley circulation. Over the Pacific Ocean precipitation is increased at aproximately 30°N and 30°S. This is connected with a pronounced split ITCZ, where both the northerly and southerly branch in the western Pacific is more intense in LGM_S than in CTL. In the Atlantic north of 45°N a large reduction in precipitation is found. This is associated with the LGM ice cover and reduced low pressure (storm track) activity in the North Atlantic.

Similarly to Boreal winter, precipitation in the Boreal summer season is generally increased in the tropics and sub-tropics. Between 30˚N and 30˚S, the increase is linked to a split ITCZ in the Pacific and with a similar feature in tropical western Atlantic. This structure has a striking resemblance to the reconstructed CLIMAP LGM SST field (not shown) and the simulated 2m temperature field (figure 5) and is likely associated with that. Precipitation has decreased in the northern flank of the equatorial belt in a region from Africa to Indonesia. This is also reflected in the zonal mean. This is a region which in modern day climate is dominated by convective weather systems and large amounts of precipitation. The substantial reduction in convective activity can be linked to the slightly reduced Hadley circulation in Boreal summer. The precipitation in the North Atlantic region in Boreal summer is also reduced in LGM_S, however to a lesser extent than in the winter season.

The geographical distribution of evaporation (not shown) in LGM_S shows similar geographical distribution as for CTL. But the evaporation has generally increased at lower latitudes and decreased at higher latitudes.

3.3 Temperature

The simulated annual global mean 2m temperature in LGM_S is 8.1ºC. This is a response to the changed boundary conditions and greenhouse gas content of -5.7K. This response is larger than the other PMIP models, which have temperature responses in the range -3.5K to -4.8K. According to figure 5 and 6,

the largest (negative) response in 2m temperature in ARPEGE is found in the northern high and mid latitudes. The ARPEGE model's temperature response to the large northern hemisphere ice sheets seems to be larger than for the PMIP ensemble (figure 6). But these regions are also where the largest spread in temperature response among the PMIP models is found. A general cooling of 2-3K in LGM_S between 30ºN and 30ºS also contributes significantly to the low global mean value due to the large area of this latitude belt. Over ocean, in general, ARPEGE simulate simulates colder temperatures than the PMIP models. The ARPEGE response is systematically 1-1.5K colder than the PMIP ensemble over ocean. Over land areas the ARPEGE response centred within the range of the PMIP models, except for over the large northern hemisphere ice sheets.

From the geographical distribution of the temperature response (figure 5), the strongest cooling is generally found over middle and high latitudes in connection with sea ice and continental ice sheets in particular. The lower latitudes are generally more homogeneously cooled.

The ARPEGE model is on the cold side compared to the other PMIP models. Closer investigation has showed that this is a response to the reduction in aerosol concentration in LGM_S. The LGM atmosphere is more transparent to solar radiation, hence less solar energy is absorbed by the atmosphere. Sensitivity experiments (not presented here) show that the reduction in atmospheric aerosols leads to ~15Wm^{-2} less absorption of solar energy in the atmosphere. This is a negative forcing and represents a cooling of the atmosphere. However, increased transparency of the atmosphere results in a larger amount of solar radiation that can be absorbed by the surface. This will in general compensate for the energy loss in the atmosphere column by increasing the heat fluxes from the ground to the atmosphere. The land areas in the model adjust accordingly to this by absorbing more solar radiation, and increasing the land surface temperatures. But since the sea surface temperatures are prescribed, increased absorption of solar radiation in the ocean does not increase the SSTs. Due to reduced atmospheric absorption of solar radiation, the atmosphere cools more than the prescribed reduction in SST from CLIMAP (1981) in tropical and subtropical ocean. This is consistent with the 1-1.5K negative bias over ocean that is found in ARPEGE.

Heat fluxes (sensible and latent) at the surface are dependent on the temperature difference between the surface and the lowest atmosphere level. Since the atmosphere cools more than the prescribed SST, this temperature difference increases and consequently heat fluxes from the surface to the atmosphere also increases. The increase in latent heat flux is consistent with the increase in evaporation and precipitation found in section 3.2.

As the zonal temperature gradient is increased, the model compensates for this by increasing the atmospheric meridional energy transport. This will help to sustain the increased fluxes of latent and sensible heat over tropical and subtropical ocean. The equilibrium reached by the model is colder throughout the lower atmosphere compared to the PMIP ensemble. In this study with prescribed SSTs, the atmosphere will not affect the state of the upper ocean in any way. A slab-ocean experiment, similar to that described by Pinot et al. (1999), would in this case be affected both by increased absorption of solar radiation in the sea surface and by the increased fluxes of latent and sensible heat. These two forcings on the sea surface has opposite sign, but the change in heat flux is larger than change in solar radiation. It would therefore be expected to develop a colder sea surface than described by the CLIMAP reconstructions at low and mid latitudes.

4 Variability at mid and high northern latitudes in LGM_S

In CTL (figure 7a) the characteristic Arctic Oscillation (AO) (e.g. Thompson and Wallace 1998) is found as the leading empirical orthogonal function (EOF) for wintertime (DJF) MSLP anomalies. The AO has three centres of action. There is one in the Pacific and one in the Atlantic, both are of approximately the same strength and sign, located at ~50ºN. The third centre of action is located in the Arctic and has opposite sign than the other two. The North Atlantic part of the AO is known as the North Atlantic Oscillation (NAO) (e.g. Wallace and Gutzler 1981). The NAO dominates the modern-day climate variability in large parts of the North Atlantic area (Trenberth and Hurrell 1994; Hurrell 1995; Dai et al.

1997; Hurrell and VanLoon 1997). The leading EOF for CTL explains 31.7% of the variability in the monthly wintertime MSLP. In LGM_S (figure 7b) the leading EOF (AO_{LGMS}) explains 26.6% of the variance in the monthly wintertime MSLP field. Following the North et al. (1982) criteria based on separation of the neighbouring eigenvalues, the leading EOF for both simulations can be regarded as significant. The North Atlantic centre of action is nearly absent in AO_{LGMS}. This indicates that the variability in the North Atlantic sector is considerably suppressed in LGM_S and corresponds thus to the nearly absent Icelandic low. The North Pacific centre of action has shifted northward and is more concentrated. Its counterpart in CTL is spread over a larger area. The concentration of this LGM action centre corresponds with the shift and strengthening of the Aleutian low in this area (figure 3).

The relation between AO/NAO and the North Atlantic storm track in modern day climate is described by Rogers (1997). The storms in the modern day North Atlantic climate are characterized by the tendency of preferring one of two track regions at a given time. One track region is in the north eastern Atlantic extending from Iceland and northeastward to the Norwegian and Barents Seas, denoted as the positive mode. The other track region is in the Bay of Biscay with cyclonic activity extending into Europe and the Mediterranean Sea, this mode is denoted the negative mode. The shift between these two modes of variability results in a split (or a broad) North Atlantic storm track in modern day climate.

A feature track algorithm (Hodges 1994; Hodges 1995; Hodges 1996; Hodges 1999) is applied on relative vorticity fields at 850 hPa. The density and intensity of synoptic low pressure trajectories (storm tracks) are analysed. As can be seen from figure 8, the density of low pressure trajectories in LGM_S is significantly different from the CTL storm track both in the Atlantic and the Pacific sector. In CTL Boreal winter the North Atlantic storm trajectories spans a broad track (figure 8a). A distinct branch of the storm track extends north-eastward towards Iceland and further into the Nordic Seas, while a southerly branch extends into the European continent. This is in good agreement with Rogers (1997) and consistent with AO_{CTL}. The corresponding North Atlantic storm track in LGM_S (figure 8b) is very zonal with a distinct narrow maximum along the ice edge. This is consistent

with the reduced North Atlantic variability evident from the AO_{LGMS}. Note that the storm track densities from CTL and LGM_S are not quantitatively comparable due to different sampling frequencies when obtaining the storm track statistics.

The North Atlantic storm track in LGM_S extends into the Eurasian continent along the southern edge of the Fennoscandian ice sheet. The Pacific storm track is shifted north and east compared to CTL, it is also broader than the Atlantic one with highest track density number found in the eastern parts along the North American west coast. This is consistent with the reduction in MSLP in this area, and the AO_{LGMS}.

LGM_S summer track density (figure 8d) in the Atlantic has similarities with the CTL winter storm track (figure 8a). A maximum is found in the Gulf of St. Laurence south of the Labrador Peninsula. It extends north-eastward along the summer ice edge toward Iceland and farther into the ice covered Nordic Seas. Summer storms are generally less intense than winter storms both in CTL and LGM_S.

5 Response to new construction of North Atlantic sea-ice cover

The second LGM experiment, LGM_N, includes revised surface conditions in the North Atlantic and the Nordic Seas as shown in figure 1. The revised reconstruction (Meland et al. 2005) represents more open waters in this region, particularly during Boreal summer. The response in any variable, χ, to more open waters in this region in LGM is defined as $\chi_{LGMN} - \chi_{LGMS}$. The response to changed surface conditions in this region has a non-local extent which is manifested in a Northern Hemisphere mid- and high latitude circulation that is more similar to modern day climate than LGM_S. The globally averaged precipitation and 2m temperature (T_{LGMN}), however, are 3.59 mm/day and 8.14ºC respectively, which is similar to the corresponding numbers in LGM_S. In examining the zonal mean structures of precipitation, T_{LGMN} and MSLP (not shown) we find close resemblance to LGM_S for both summer and winter, except

in northern mid- and high latitudes. At the latitudes north of 50ºN, higher temperatures are evident in LGM_N, with a maximum anomaly of 2K zonally at 60ºN in Boreal winter. Boreal summer has a somewhat less pronounced anomaly of 0.5K. The pressure is in general increased south of 50ºN in both seasons, while decreased north of 50ºN.

5.1 Northern Hemisphere response in Boreal winter

The main feature of the simulated response in LGM to open waters in the Nordic Seas is seen as a warm low pressure anomaly (figure 9a) that extends, with lower amplitude, in a semi-circle from the Nordic Seas along the 60ºN latitude over the Eurasian continent and to the Bering Strait. It has a latitudinal width of about 20º. The maximum MSLP amplitude is 5hPa over the area of perturbed sea-ice. South of the semi-circle shaped anomaly, a general increase in MSLP with a peak in the eastern parts of the Pacific and Atlantic is found. This pressure increase does not seem connected with any systematic change in other parameters. The 2m temperature response (figure 9b) is more than 10K over the Nordic Seas and decreases rapidly to ~2K in the rest of the core of the semi-circle shaped anomaly. The precipitation response (figure 9c) has a similar shape as the other two surface parameters, but is relatively seen weaker outside the Nordic Seas. Precipitation has increased by more than 200%, equivalent to 2-3 mm/day, south of Iceland. This is a direct response to the reduced sea ice cover. Over the Fennoscandian ice sheet only a minor increase in precipitation is found, about 20%. This is less than 0.25mm/day. A 40-60% decrease in precipitation (equivalent to 2-3mm/day) and a negative temperature anomaly of 3-4K is found in Eastern Siberia and Bering Sea.

The Icelandic low is strengthened in LGM_N, which is evident in figure 9a. A maximum decrease in pressure south of Iceland is consistent with the open water and warmer boundary conditions locally (SST) in the new reconstruction. This suggests that the Icelandic low in parts is thermally forced or generated as an atmosphere-ocean coupled process by transfer of heat and moisture from the ocean to the atmosphere.

Figure 10 shows a vertical cross-section longitudinally along 60ºN. Temperature response is plotted in colours and the geopotential height is plotted as solid and dotted contours. The local warm anomaly from the changed North Atlantic/Nordic Seas surface conditions reaches up to the 500hPa level. At higher levels the response is negative. The height field responds with a low level trough at the location of the thermal forcing below 800hPa, while an increase of 30m is evident in the upper troposphere. This configuration generates an upper tropospheric wave pattern which can be seen as alternating series of positive and negative height anomalies at the 200hPa level shown in figure 11a. This will be explained in section 5.3.

5.2 Northern Hemisphere response in Boreal summer

The summer response in near-surface parameters is more local, particularly for temperature and precipitation (figures 12b,c). A warm anomaly (up to 3K) is located in the Nordic Seas and a cold anomaly (~2K) west of Ireland. According to figure 12c precipitation anomalies with same sign and location is found as well. The MSLP response (figure 12a) has a larger scale and is dominated by a weak (~1-2hPa) low pressure anomaly in the Arctic region with some southward extensions over the northern continents. A large reduction in MSLP is found in the north western Pacific Ocean. Except from the anomaly over east Siberia, the response in MSLP in Boreal summer is not statistically significant. Precipitation increases by nearly 100%, equivalent to 0.5 mm/day, in the Nordic Seas in Boreal summer. Over Scandinavia, and the Fennoscandian Ice sheet, no change in precipitation is found.

The most pronounced features in the mid- and upper tropospheric temperature and geopotential fields are located over eastern Siberia. A warm anomaly of 2-3K is found in the 850hPa temperature field (not shown). This anomaly strengthens towards the surface where the maximum response reaches 5K (figure 12b). Response in the geopotential fields is also evident at this geographical location. The geopotential height field at 850hPa shows only a relatively weak response, while the anomaly becomes far stronger in the upper troposphere with a maximum

of 40m at the 200hPa level. This is probably connected with the wave pattern that can be seen in the 200hPa level geopotential field in Boreal summer (figure 11b).

5.3 Mechanisms and changes in variability

The strongest simulated response to the perturbed boundary conditions is found during the Boreal winter. At the latitudes that are directly influenced by the change in sea ice cover and SSTs, the winter season is dominated by the baroclinic zone where cold polar air meets warmer subtropical air. This favours higher synoptic winter activity and thus a larger number of synoptic storms with higher intensity than observed in the summer season. The contrast between the air and surface when the polar air flows over open ocean is less in summer than in winter. The baroclinicity is also smaller, thus weaker and fewer low pressure systems are generated. The atmospheric variability during summer is lower and we thus see only local effects from the reduced sea ice cover.

The local response to the reduced sea ice cover is small in Boreal summer (3K) compared to Boreal winter (>10K). During the winter season the sea ice acts as a lid that suppresses the heat transport from the ocean to the atmosphere. The temperature of the ice surface is dependent on the radiative processes and turbulent energy exchange with the atmosphere. The low intensity of solar radiation and high albedo leads to cold surface temperatures on the sea ice in the winter season. In the summer season solar radiation will heat the sea ice surface and surface melting will occur. Melt ponds will form and more solar radiation can be absorbed by the surface due to reduced sea ice albedo in the summer. The sea ice temperatures are higher in the summer and are close to the melting point of the ice. Consequently the local temperature response to changed sea ice cover is quite small in summer compared to winter over the Nordic Seas.

The linear response to a number of thermal forcings has been studied by Hoskins and Karoly (1981) by using a linearized steady-state 5-layer baroclinic model. They found that the perturbation generated wave patterns on the sphere, depending on the location, shape and vertical distribution of the heating. A

thermal anomaly in the mid-latitudes is generally balanced by horizontal temperature advection, independent of the vertical distribution of the heating.

By introducing a shallow, circular heat source at 60ºN in their model, and applying a westerly zonal flow, a surface low with an anomaly of 22.1hPa was generated 15º east of the heating source. Such an anomaly sets up a northerly flow that brings cold polar air southward over the anomaly. The creation of vorticity associated with the meridional movement must be balanced by a downward motion over the heat source. In this way higher temperatures are found east of the area of maximum heating. The heating anomaly generates a wave pattern in the upper troposphere, which is seen as alternating series of positive and negative height anomalies. The direction of these wave trains is dependent on the wavelength of the generated wave as well as of the zonal wind speed and meridional location of the heating source. Waves with longer wavelengths tend to propagate poleward, while shorter waves propagate equatorward.

The reduced sea ice cover in Meland et al's reconstruction represents a heat source in Boreal winter centred at 15°W (figure 10a). The low level trough and reduction in MSLP are evident. Above the heating anomaly an increase in geopotential is found. The thickness in the 1000-200hPa layer is increased by 60m in LGM_N at this location. This in turn seems to generate a zonal wave pattern, with alternating positive and negative anomalies longitudinally.

This response in 200hPa height (figure 11a) clearly shows a wave structure that resembles what is described by Hoskins and Karoly (1981). A positive height anomaly is found directly above the heating source. A wave propagates nearly zonally 180º from the source, where it seems to split and propagate equatorward. Such a response in geopotential is also similar to what is found by Kushnir et al. (2002). Also to be noted is the large negative geopotential response at around 180º. This seems to penetrate down to the surface and create the above mentioned cooling near the surface over eastern Siberia. The statistical confidence of the described pattern is relatively weak. It is significantly different from zero at the 10% level only over Scandinavia, Northeast Pacific and over North America.

The atmospheric response to the JJA forcing is more difficult to interpret. The cross-section at 60ºN (figure 10b) show only minor evidence of heating from the reduced sea ice cover (less than 1K response). Only the lowest model levels are affected by the change in boundary conditions. However a large heating anomaly is evident over Eastern Siberia. The geopotential height anomaly over eastern Siberia is positive in the upper troposphere and has a low level trough. This anomaly reaches higher in to the atmosphere than the one over the perturbed areas and amplifies with increasing height. It has a larger spatial extent and is stronger in amplitude than the DJF counterpart. A wave structure is apparent over eastern Siberia during JJA (figure 11b). But the damping of the wave is larger than in DJF. The positive height anomaly over Eastern Siberia and the negative height anomaly over North America are significantly different from zero at the 5% level. The different wave patterns indicate that different mechanisms or variability modes are active in the two seasons in LGM_N. This may possibly be a result of non-linear effects and feedback mechanisms.

Differences in the North Atlantic storm track in Boreal winter are found in LGM_N (figure 13). The storm track is shifted northward along the North American east coast. The storm track over the Atlantic has become somewhat wider. It is not restricted in the same degree by the sea ice edge as in LGM_S. This also suggests higher degree of variability. Storm track density is increased from Iceland, over the Fennoscandian ice sheet and further into Russia and Siberia. The number of storm tracks increases over Southern Siberia or Mongolia, while the north Pacific storm track is reduced. A reduction is found on the Siberian side of the Arctic Ocean, while an increase is found over the Aleutians, Bering Strait and the American side of the Arctic Ocean.

The North Atlantic Oscillation pattern is again evident in the leading mode of variability for monthly wintertime MSLP (not shown). The North Atlantic centre of action is still weaker and is displaced southwestward compared to CTL. Our results indicate that the NAO signal is in large parts driven by the energy transfer from the ocean to the atmosphere in the North Atlantic Ocean.

In Boreal summer the responses in storm tracks are generally weaker than in Boreal winter. Storm tracks decrease over the North American continent at around 40-50°N and increase north of 50°N (figure 13b). An increase in summer storms is also evident over eastern Siberia. The intensity (not shown) of the storm tracks remain more or less the same in LGM_N as in LGM_S.

The increase in winter storm tracks in the North Atlantic in LGM_N will carry larger amounts heat and moisture into Scandinavia. This is also evident from figures 9b,c. The open ocean in LGM_N west of Ireland during winter is a source of heat and moisture to the atmosphere. There are close similarities between the storm track and temperature anomalies during the winter season. The increased number of storm tracks from Scandinavia into Russia and Siberia bring more heat into the area, and contribute thus to increase the Siberia winter temperature by 1-2ºC. The moisture in the storms is more quickly released as they reach the edges of the sea ice or ice sheets. Only a minor increase in precipitation over the ice-sheets is found. The low temperatures and high elevation of the ice sheets can only sustain air with small amounts of moisture. In our experiment the air is cooled and the moisture precipitates along the ice sheet edges when the flow enters this region.

6 Conclusions

Two simulations of the Last Glacial Maximum were performed with the atmosphere general circulation model, ARPEGE, in addition to a control simulation of modern day climate. The first LGM simulation, LGM_S, was a standard PMIP run with SST boundary conditions given by CLIMAP (1981). For the second LGM simulation, LGM_N, the SST reconstructions of Meland et al. (2005) were used as a basis for the boundary conditions.

Comparison with corresponding LGM simulations from PMIP shows qualitatively the same structures in LGM_S. But the ARPEGE model is generally colder than the PMIP ensemble and simulates increased precipitation in LGM_S compared to CTL. The atmosphere cools more than the prescribed SSTs in LGM_S, and thus increases the surface fluxes of heat and moisture. This in combination with a strengthened

Hadley circulation explains the larger amounts of precipitation found in LGM_S at lower latitudes.

The mean response to the new SST reconstruction is seen as a heating anomaly with increased temperatures locally over the northern North Atlantic. The increased energy exchange from the open ocean to the atmosphere at this location also increases evaporation and precipitation locally and the sea level pressure is reduced. This heating anomaly during Boreal winter gives a response not only locally, but also as an upper tropospheric wave forcing which has the potential to carry the signal over large distances. Such a teleconnection pattern is found as a response to the reduced sea ice cover in LGM_N, and is consistent with the linear response described by Hoskins and Karoly (1981).

The study reveals some interesting features concerning large scale and synoptic variability with focus on the North Atlantic. The Icelandic low is clearly suppressed in LGM climate. In LGM_S the Icelandic low totally disappears (figure 3a). The area of ice-free waters south of Iceland during winter in LGM_N make the Icelandic low re-appear, although weaker than in modern day climate (figure 9a). The Icelandic low is in ARPEGE dependent on the marine supply of latent and sensible heat. The analysis of the variability in the North Atlantic shows the same dependence on the ice-free waters. AO_{LGMS} differs significantly from AO_{CTL} as the North Atlantic centre of action is not apparent in the EOF analysis of monthly wintertime sea level pressure for LGM_S. In LGM_N, however, variability in the North Atlantic is again strengthened.

This response in the main variability mode is associated with a characteristic change in storm tracks. The storms clearly follow the zonally oriented sea ice edge in LGM_S, while a wider range of paths is apparent in LGM_N. The synoptic variability is profoundly altered by the altered reconstruction of sea ice and SST. A larger number of storms are apparent over the Fennoscandian ice sheet in LGM_N than in LGM_S. This has the potential to bring larger amounts of heat and moisture to the ice sheet.

When the Meland et al.(2005) reconstruction is applied instead of the CLIMAP (1981) reconstruction, evaporation and precipitation (figure 9c and 12c) increase as a direct response to the increased air-sea interaction allowed by the reduced sea ice cover. More moisture is supplied to the air in LGM_N, consistent with the current understanding of the rapid growth of the Fennoscandian and Barents Ice Sheets during LGM (Boulton 1979; Elverhoi et al. 1995; Mangerud et al. 2002). The growth clearly requires a strong source of precipitation, and a degree of meridional transport. A zonal circulation, which is the result when using the CLIMAP (1981) reconstruction as boundary conditions, may provide too little winter precipitation to feed rapid growth of ice sheets in the northern portion of the Nordic Seas.

Acknowledgements

This work has been supported by Faculty of Mathematics and Natural Sciences, University of Bergen and by MACESIZ, Marine Climate and Ecosystems in the Seasonal Ice Zone, founded by the Research Council of Norway. This is publication number A 112 from the Bjerknes Centre for Climate Research.

References

Bentsen M, Drange H, Furevik T, Zhou T (2004) Simulated variability of the Atlantic meridional overturning circulation. Clim Dynam 22: 701-720

Bonfils CJ, Lewden D, Taylor KE (1998) Documentation of the PMIP models. PCMDI Report

Boulton GS (1979) Glacial History Of The Spitsbergen Archipelago And The Problem Of A Barents Shelf Ice Sheet. Boreas 8: 31-57

CLIMAP (1981) Seasonal reconstruction of the Earth's surface at the Last Glacial Maximum. Map Chart Series MC-36

Dai A, Fung IY, DelGenio AD (1997) Surface observed global land precipitation variations during 1900-88. J Climate 10: 2943-2962

de Vernal A, Hillaire-Marcel C, Turon JL, Matthiessen J (2000) Reconstruction of sea-surface temperature, salinity, and sea-ice cover in the northern North Atlantic during the last glacial maximum based on dinocyst assemblages. Can J Earth Sci 37: 725-750

Denton GH, Hughes TJ, Eds. (1981). The Last great ice sheets. A Wiley-Interscience publication, New York, 484pp

Deque M, Dreveton C, Braun A, Cariolle D (1994) The Arpege/Ifs Atmosphere Model - A Contribution To The French Community Climate Modeling. Clim Dynam 10: 249-266
Deque M, Marquet P, Jones RG (1998) Simulation of climate change over Europe using a global variable resolution general circulation model. Clim Dynam 14: 173-189
Deque M, Piedelievre JP (1995) High-Resolution Climate Simulation Over Europe. Clim Dynam 11: 321-339
Dong B, Valdes PJ (1998) Simulations of the Last Glacial Maximum climates using a general circulation model: prescribed versus computed sea surface temperatures. Clim Dynam 14: 571-591
Elverhoi A, Svendsen JI, Solheim A, Andersen ES, Milliman J, Mangerud J, Hooke RL (1995) Late Quaternary Sediment Yield From The High Arctic Svalbard Area. J Geol 103: 1-17
Hall NMJ, Valdes PJ, Dong BW (1996) The maintenance of the last great ice sheets: A UGAMP GCM study. J Climate 9: 1004-1019
Hebbeln D, Dokken T, Andersen ES, Hald M, Elverhoi A (1994) Moisture Supply For Northern Ice-Sheet Growth During The Last-Glacial-Maximum. Nature 370: 357-360
Hodges KI (1994) A General-Method For Tracking Analysis And Its Application To Meteorological Data. Mon Weather Rev 122: 2573-2586
Hodges KI (1995) Feature Tracking On The Unit-Sphere. Mon Weather Rev 123: 3458-3465
Hodges KI (1996) Spherical nonparametric estimators applied to the UGAMP model integration for AMIP. Mon Weather Rev 124: 2914-2932
Hodges KI (1999) Adaptive constraints for feature tracking. Mon Weather Rev 127: 1362-1373
Hoskins BJ, Karoly DJ (1981) The Steady Linear Response Of A Spherical Atmosphere To Thermal And Orographic Forcing. J Atmos Sci 38: 1179-1196
Hurrell JW (1995) Decadal Trends In The North-Atlantic Oscillation - Regional Temperatures And Precipitation. Science 269: 676-679
Hurrell JW, VanLoon H (1997) Decadal variations in climate associated with the north Atlantic oscillation. Climatic Change 36: 301-326
Joussaume S, Taylor KE (1995) Status of the Paleoclimate Modeling Intercomparison Project (PMIP). Proceedings of the first international AMIP scientific conference. WCRP Report: 425-430
Joussaume S, Taylor KE (2001) The Paleoclimate Modelling Intercomparison Project. Proceedings of the third PMIP Workshop. WCRP 111
Kushnir Y, Robinson WA, Blade I, Hall NMJ, Peng S, Sutton R (2002) Atmospheric GCM response to extratropical SST anomalies: Synthesis and evaluation. J Climate 15: 2233-2256
Kutzbach JE (1988) Climatic Changes Of The Last 18,000 Years - Observations And Model Simulations. Science 241: 1043-1052
Lautenschlager M, Herterich K (1990) Atmospheric Response To Ice-Age Conditions - Climatology Near The Earths Surface. J Geophys Res-Atmos 95: 22547-22557
Mangerud J, Astakhov V, Svendsen JI (2002) The extent of the Barents-Kara Ice Sheet during the Last Glacial Maximum. Quaternary Sci Rev 21: 111-119
Meland MY, Jansen E, Elderfield H (2005) Constraints on SST estimates for the northern North Atlantic/Nordic Seas during the LGM. Quaternary Sci Rev 24 (7-9): 835-852
North GR, Bell TL, Cahalan RF, Moenig FJ (1982) Sampling errors in the stimation of empirical orthogonal functions. Mon Wea Rev 110: 699-706
Peltier WR (1994) Ice-Age Paleotopography. Science 265: 195-201
Pflaumann U, Duprat J, Pujol C, Labeyrie LD (1996) SIMMAX: A modern analog technique to deduce Atlantic sea surface temperatures from planktonic foraminifera in deep-sea sediments. Paleoceanography 11: 15-35

Pflaumann U, Sarnthein M, Chapman M, d'Abreu L, Funnell B, Huels M, Kiefer T, Maslin M, Schulz H, Swallow J, van Kreveld S, Vautravers M, Vogelsang E, Weinelt M (2003) Glacial North Atlantic: Sea-surface conditions reconstructed by GLAMAP 2000. Paleoceanography 18

Pinot S, Ramstein G, Marsiat I, de Vernal A, Peyron O, Duplessy JC, Weinelt M (1999) Sensitivity of the European LGM climate to North Atlantic sea-surface temperature. Geophys Res Lett 26: 1893-1896

Reynolds RW, Smith TM (1995) A High-Resolution Global Sea-Surface Temperature Climatology. J Climate 8: 1571-1583

Rogers JC (1997) North Atlantic storm track variability and its association to the north Atlantic oscillation and climate variability of northern Europe. J Climate 10: 1635-1647

Rosell-Mele A, Comes P (1999) Evidence for a warm Last Glacial Maximum in the Nordic seas or an example of shortcomings in U-37(K)' and U-37(K) to estimate low sea surface temperature? Paleoceanography 14: 770-776

Sarnthein M, Jansen E, Weinelt M, Arnold M, Duplessy JC, Erlenkeuser H, Flatoy A, Johannessen G, Johannessen T, Jung S, Koc N, Labeyrie L, Maslin M, Pflaumann U, Schulz H (1995) Variations In Atlantic Surface Ocean Paleoceanography, 50-Degrees-80-Degrees-N - A Time-Slice Record Of The Last 30,000 Years. Paleoceanography 10: 1063-1094

Shin SI, Liu Z, Otto-Bliesner B, Brady EC, Kutzbach JE, Harrison SP (2003) A simulation of the last glacial maximum climate using the NCAR-CCSM. Clim Dynam 20: 127-151

Thompson DWJ, Wallace JM (1998) The Arctic Oscillation signature in the wintertime geopotential height and temperature fields. Geophys Res Lett 25: 1297-1300

Trenberth KE, Hurrell JW (1994) Decadal Atmosphere-Ocean Variations In The Pacific. Clim Dynam 9: 303-319

Veum T, Jansen E, Arnold M, Beyer I, Duplessy JC (1992) Water Mass Exchange Between The North-Atlantic And The Norwegian Sea During The Past 28,000 Years. Nature 356: 783-785

Wagner T, Henrich R (1994) Organo- and lithofacies of TOC-lead glacial/interglacial deposits in the Norwegian-Greenland Sea: sedimentary and diagenetic responses to paleoceanographic and paleoclimatic changes. Mar Geology 120: 335-364

Wallace JM, Gutzler DS (1981) Teleconnections In The Geopotential Height Field During The Northern Hemisphere Winter. Mon Weather Rev 109: 784-812

Weinelt M, Sarnthein M, Pflaumann U, Schulz H, Jung SJA, Erlenkeuser H (1996) Ice-free Nordic Seas during the Last Glacial Maximum? Potential sites of deepwater formation. Paleoclimates 1: 283-309

Figure 1: Upper left figure (a) shows the CLIMAP LGM reconstruction of SST for February and upper right figure (b) shows the new LGM reconstruction of SST for February. Lower left (c) and lower right (d) is the same as (a) and (b) but for August. Units are ºC, contour lines are drawn for every ºC. The sea ice edge is drawn as a thicker contour at -0.5ºC. Continental ice sheets are displayed in light shading and land area in dark shading. Modern day land contours are also drawn.

Figure 2: The black curve is the difference between annual zonal mean sea level pressure for LGM_S and CTL in ARPEGE. An ensemble of 9 other models (light shaded curves) is plotted for comparison.

Figure 3: Response (LGM_S-CTL) in mean sea level pressure for a) Boreal winter (upper), b) Boreal summer (lower). Units are in hPa and contours are drawn every 2.5hPa. Positive response is drawn in solid curves, negative response is drawn in dashed curves. All anomalies shown are significantly different from zero at the 1% level.

Figure 4: Change in precipitation (LGM_S-CTL), upper (a) is Boreal winter, lower (b) is Boreal summer. Units are mm/day.

Figure 5: Annual difference in 2m temperature between LGM_S and CTL. Units are °C. Color contours are drawn every 5°C. White contours are drawn every °C in the range -5°C to 3°C.

Figure 6: Zonal annually averaged 2m temperature difference between LGM_S and CTL. The units are ºC. The 9 PMIP models are plotted in light shaded colour while the ARPEGE run is plotted in black.

Figure 7: Left figure (a) is the leading EOF for CTL, based on monthly wintertime MSLP for 15 years of integration. Right figure (b) is the leading EOF for LGM_S based on monthly averaged SLP for the 10 last winters of the integrations. Units are hPa, contours are drawn every hPa. Dashed and solid lines are variability of opposite sign.

Figure 8: Density of low pressure trajectories. Upper left (a) for Boreal winter in CTL, upper right (b) for Boreal winter in LGM_S, lower left (c) for Boreal summer in CTL, lower right (d) for Boreal summer in LGM_S. The units are normalized values on a spherical domain.

Figure 9: Response LGM_N-LGM_S in Boreal winter for a) MSLP [hPa] b) 2m temperature [°C] and c) precipitation [%]. The grey contours in a and b show the regions significantly different from zero at the 5% level.

Figure 10: Vertical crossection of temperature response and response in geopotential height zonally along 60ºN. Upper figure (a) is Boreal winter, lower figure (b) is Boreal summer. The colours denote response (LGM_N - LGM_S) in temperature given as K on the colourbar on the right.

Solid curves represent an increase in geopotential height; dotted curves represent a reduction in geopotential height. Contours are drawn every 5m. Pressure level in hPa is given on the Y-axis, while longitude is given on the X-axis.

Figure 11: Response (LGM_N - LGM_S) in geopotential height at the 200 hPa level. Left figure (a) is the response for Boreal winter, right figure (b) is the response for Boreal summer. Contour lines are drawn every 5m. Increase in geopotential height is plotted in solid curves, while a reduction is plotted in dashed curves.

Figure 12: Response LGM_N-LGM_S in Boreal summer for a) MSLP [hPa] b) 2m temperature [°C] and c) precipitation [%].The grey contours in a and b show the regions significantly different from zero at the 5% level.

Figure 13: Response (LGM_N - LGM_S) in storm track density. Left figure (a) is Boreal winter. Right figure (b) is Boreal summer. Units are %.

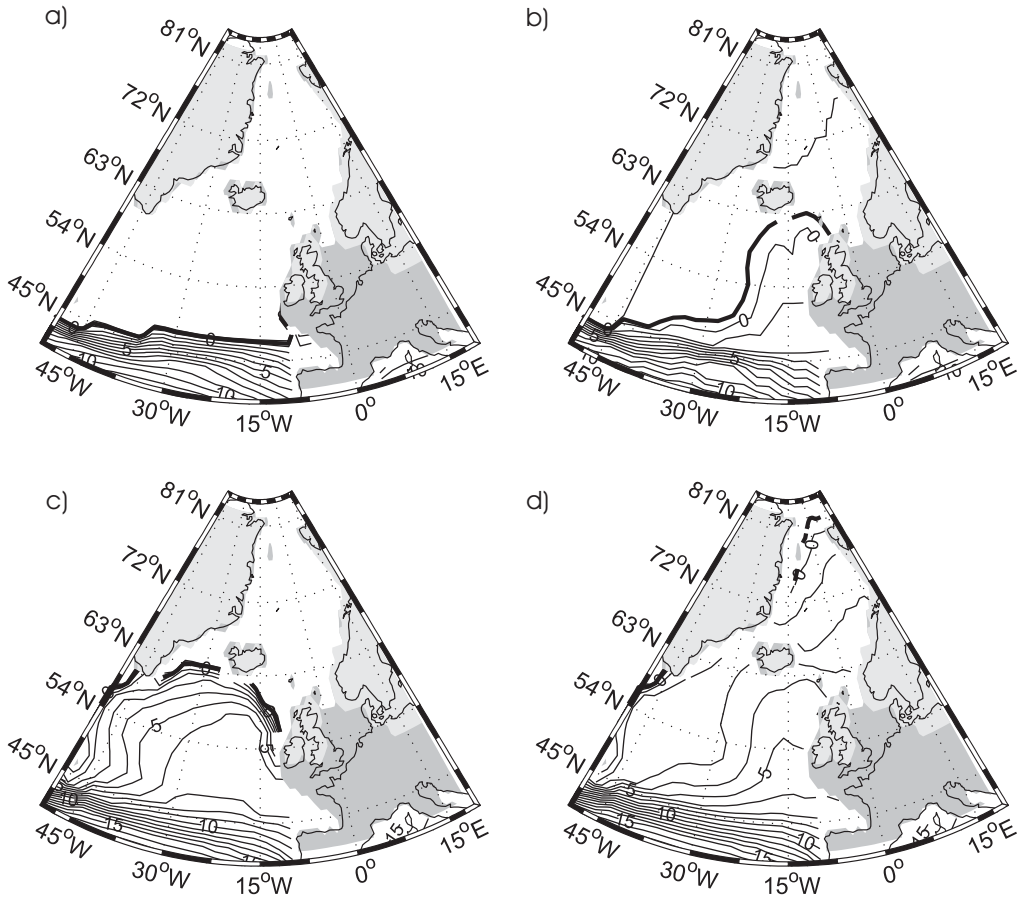

Figure 1: Upper left figure (a) shows the CLIMAP LGM reconstruction of SST for February and upper right figure (b) shows the new LGM reconstruction of SST for February. Lower left (c) and lower right (d) is the same as (a) and (b) but for August. Units are ºC, contour lines are drawn for every ºC. The sea ice edge is drawn as a thicker contour at -0.5ºC. Continental ice sheets are displayed in light shading and land area in dark shading. Modern day land contours are also drawn.

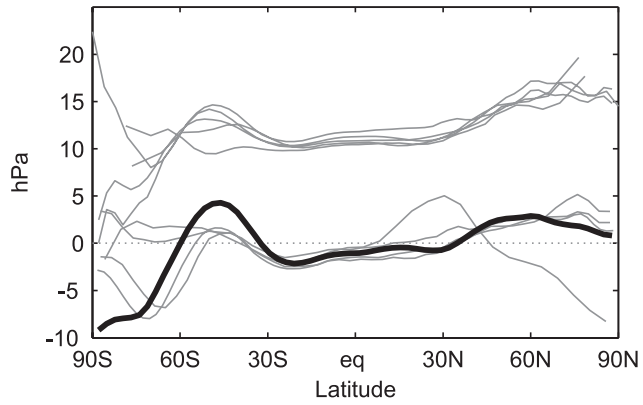

Figure 2: The black curve is the difference between annual zonal mean sea level pressure for LGM_S and CTL in ARPEGE. An ensemble of 9 other models (light shaded curves) is plotted for comparison.

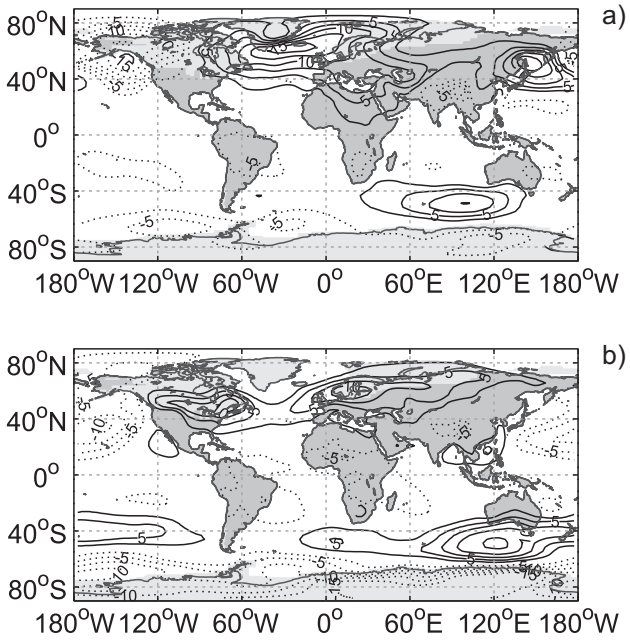

Figure 3: Response (LGM_S-CTL) in mean sea level pressure for a) Boreal winter (upper), b) Boreal summer (lower). Units are in hPa and contours are drawn every 2.5hPa. Positive response is drawn in solid curves, negative response is drawn in dashed curves. All anomalies shown are significantly different from zero at the 1% level.

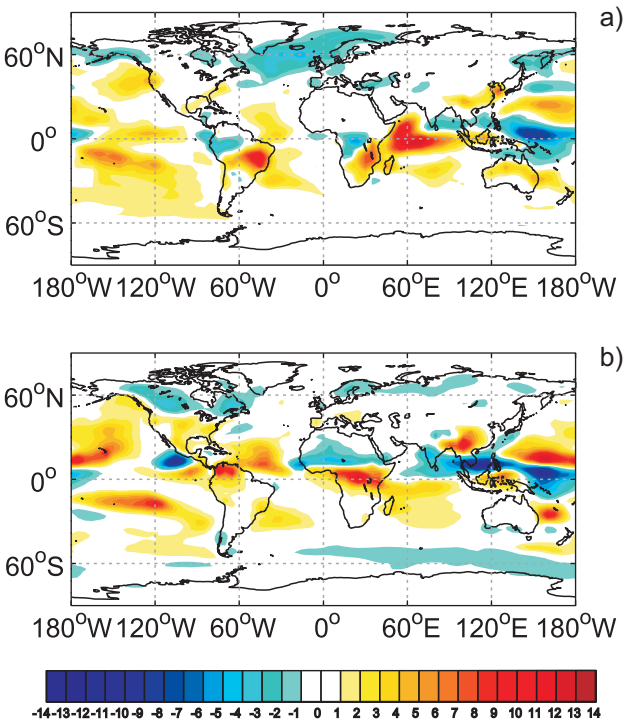

Figure 4: Change in precipitation (LGM_S-CTL), upper (a) is Boreal winter, lower (b) is Boreal summer. Units are mm/day.

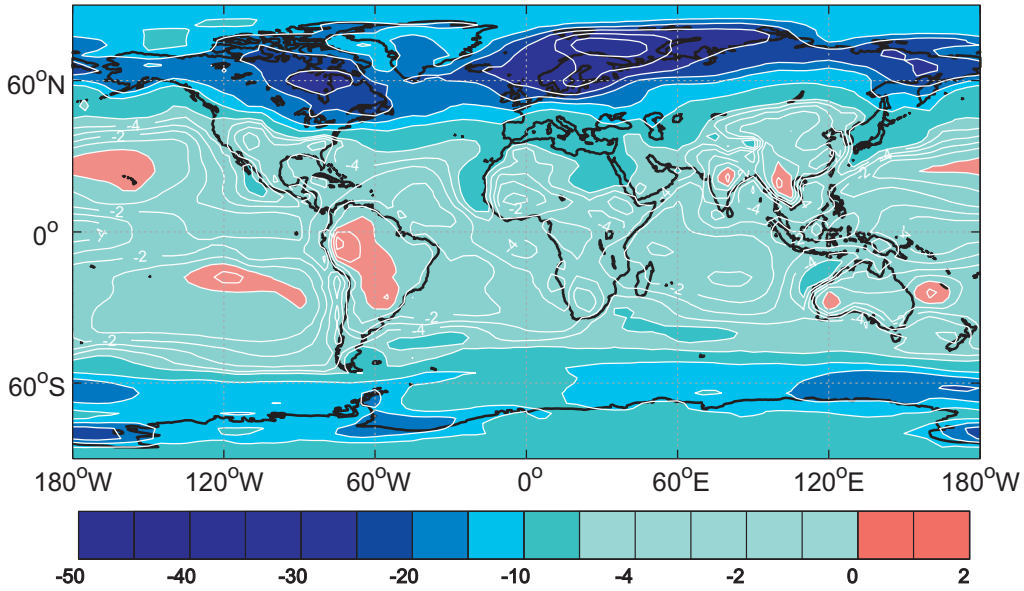

Figure 5: Annual difference in 2m temperature between LGM_S and CTL. Units are °C. Color contours are drawn every 5°C. White contours are drawn every °C in the range -5°C to 3°C.

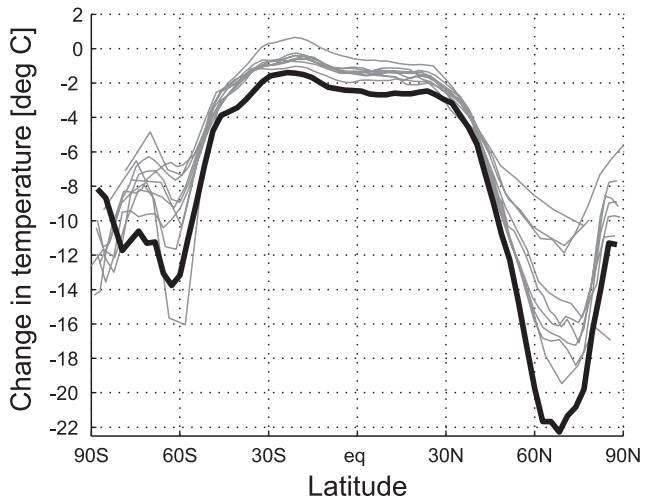

Figure 6: Zonal annually averaged 2m temperature difference between LGM_S and CTL. The units are ºC. The 9 PMIP models are plotted in light shaded colour while the ARPEGE run is plotted in black.

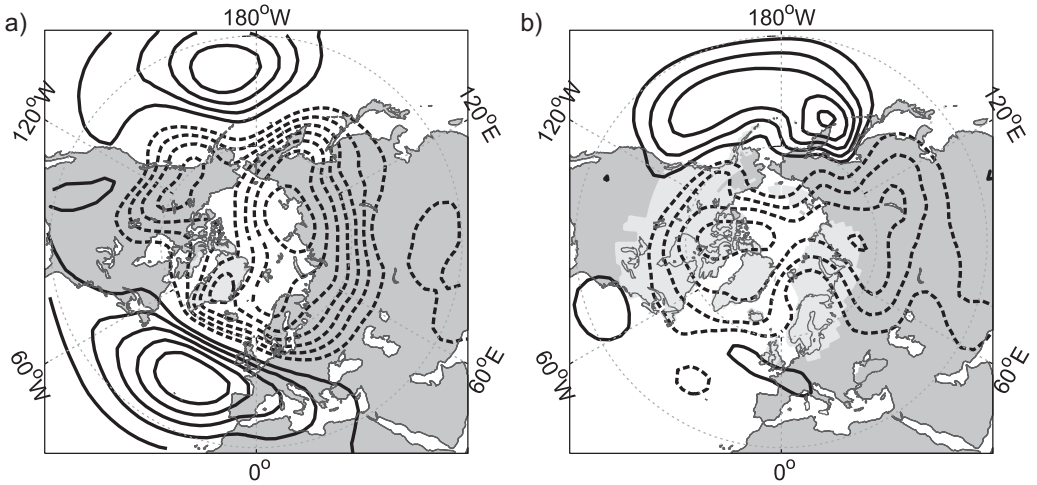

Figure 7: Left figure (a) is the leading EOF for CTL, based on monthly wintertime MSLP for 15 years of integration. Right figure (b) is the leading EOF for LGM_S based on monthly averaged SLP for the 10 last winters of the integrations. Units are hPa, contours are drawn every hPa. Dashed and solid lines are variability of opposite sign.

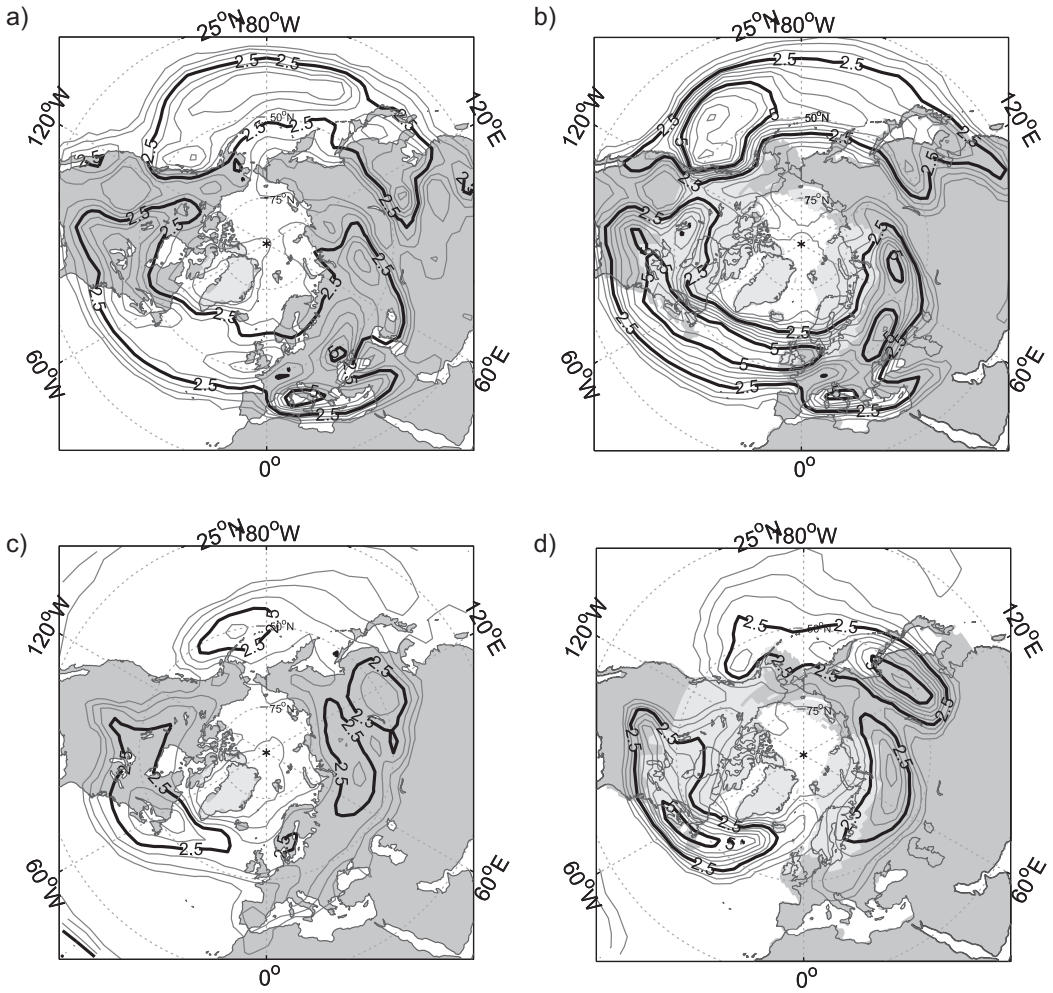

Figure 8: Density of low pressure trajectories. Upper left (a) for Boreal winter in CTL, upper right (b) for Boreal winter in LGM_S, lower left (c) for Boreal summer in CTL, lower right (d) for Boreal summer in LGM_S. The units are normalized values on a spherical domain.

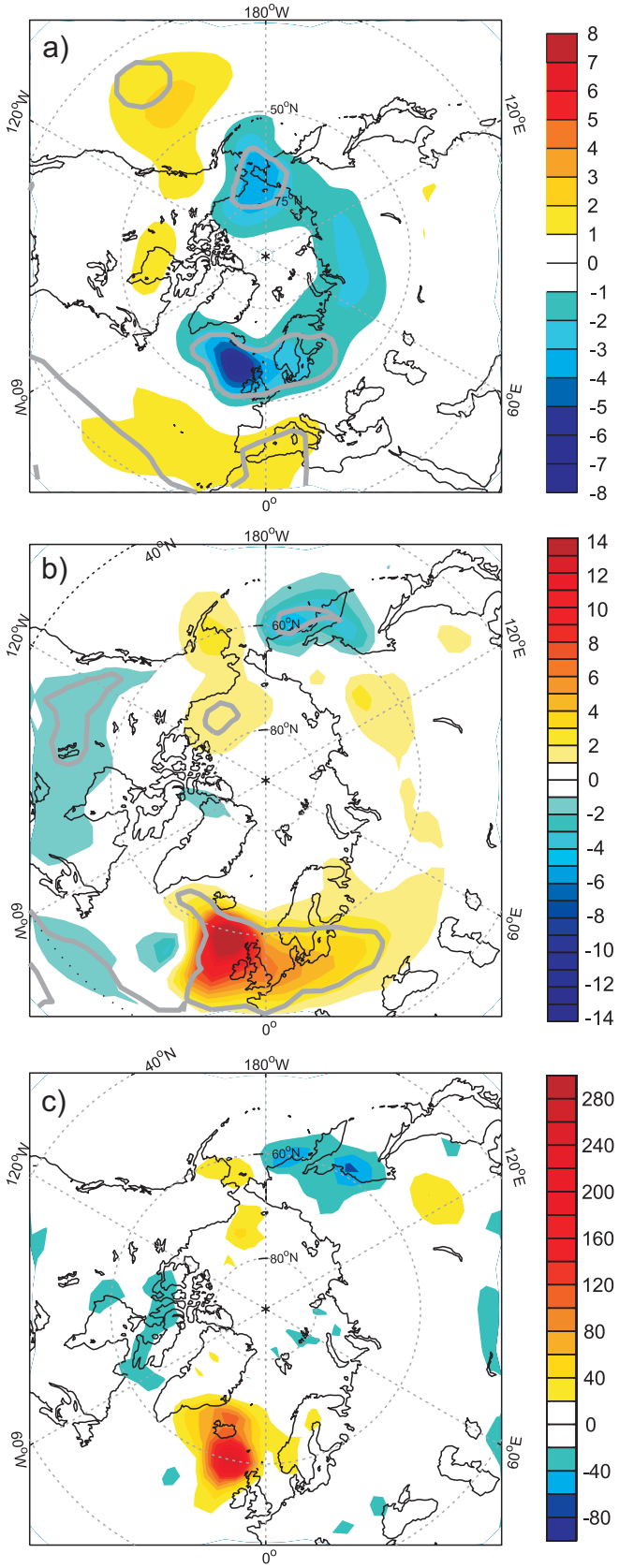

Figure 9: Response LGM_N-LGM_S in Boreal winter for a) MSLP [hPa] b) 2m temperature [°C] and c) precipitation [%]. The grey contours in a and b show the regions significantly different from zero at the 5% level.

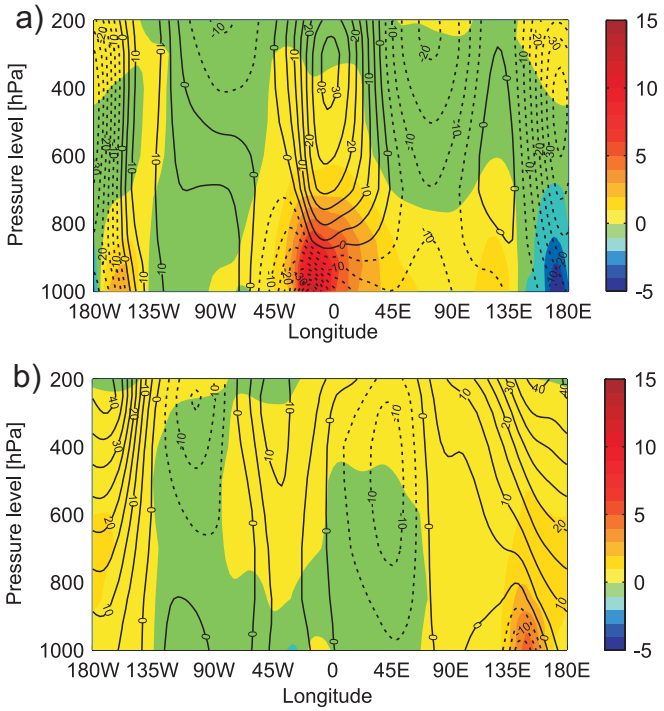

Figure 10: Vertical crossection of temperature response and response in geopotential height zonally along 60ºN. Upper figure (a) is Boreal winter, lower figure (b) is Boreal summer. The colours denote response (LGM_N - LGM_S) in temperature given as K on the colourbar on the right. Solid curves represent an increase in geopotential height; dotted curves represent a reduction in geopotential height. Contours are drawn every 5m. Pressure level in hPa is given on the Y-axis, while longitude is given on the X-axis.

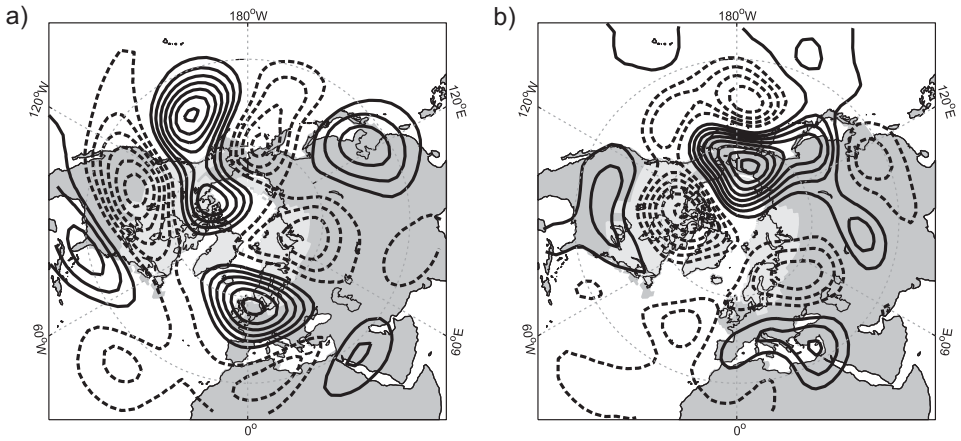

Figure 11: Response (LGM_N - LGM_S) in geopotential height at the 200 hPa level. Left figure (a) is the response for Boreal winter, right figure (b) is the response for Boreal summer. Contour lines are drawn every 5m. Increase in geopotential height is plotted in solid curves, while a reduction is plotted in dashed curves.

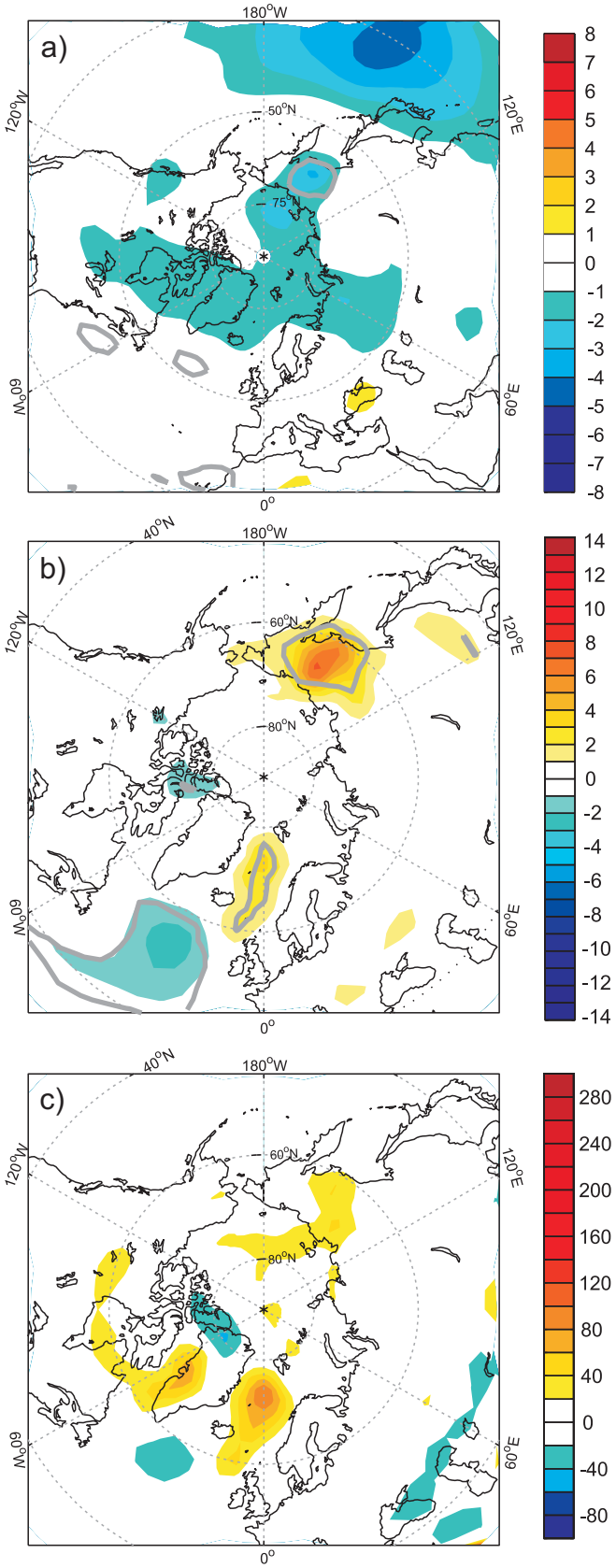

Figure 12: Response LGM_N-LGM_S in Boreal summer for a) MSLP [hPa] b) 2m temperature [°C] and c) precipitation [%].The grey contours in a and b show the regions significantly different from zero at the 5% level.

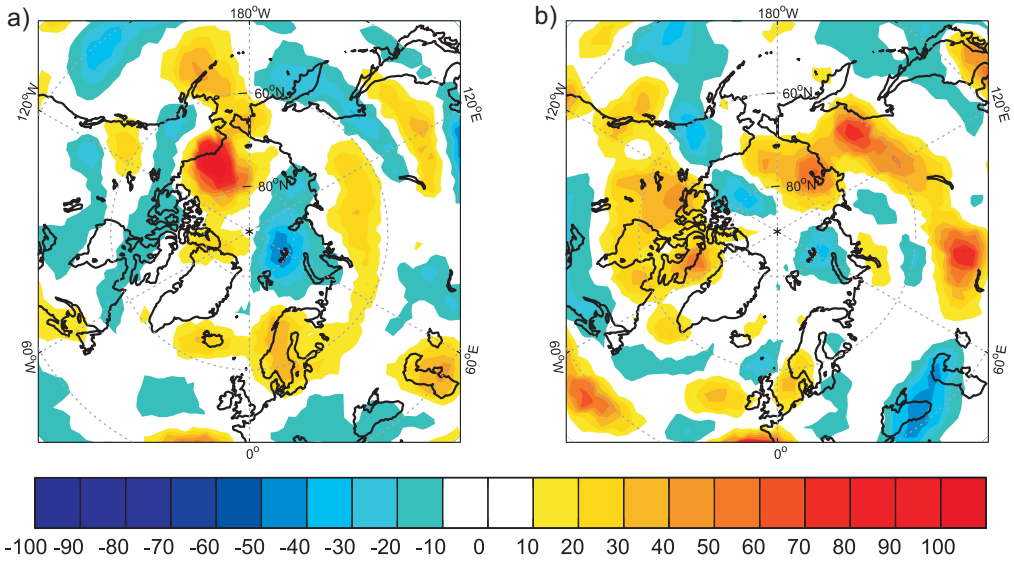

Figure 13: Response (LGM_N - LGM_S) in storm track density. Left figure (a) is Boreal winter. Right figure (b) is Boreal summer. Units are %.